PAPER

Check for updates

Catalytic effect of transition metal-doped medical grade polymer on *S*-nitrosothiol decomposition and its biological response

Arnab Mondal, [ID] [a] Patrick Maffe,[a] Sarah N. Wilson,[a] Sama Ghalei, [ID] [a] Ricky Palacio,[a] Hitesh Handa [ID] [ab] and Elizabeth J. Brisbois [ID] *[a]

Nitric oxide (NO)-release from polymer metal composites is achieved through the incorporation of NO donors such as *S*-nitrosothiols (RSNO). Several studies have shown that metal nanoparticles catalytically decompose RSNO to release NO. In polymer composites, the NO surface flux from the surface can be modulated by the application of metal nanoparticles with a varying degree of catalytic activity. In this study, we compare the NO-releasing polymer composite design strategy – demonstrating how different ways of incorporating RSNO and metal nanoparticles can affect NO flux, donor leaching, or biological activity of the films. The first approach included blending both the RSNO and metal nanoparticle in the matrix (non-layered), while the second approach involved dip-coating metal nanoparticle/polymer layer on the RSNO-containing polymer composite (layered). Secondly, we compare both designs with respect to metal nanoparticles, including iron (Fe), copper (Cu), nickel (Ni), zinc (Zn), and silver (Ag). Differential NO surface flux is observed for each metal nanoparticle, with the Cu-containing polymer composites showing the highest flux for layered composites, whereas Fe demonstrated the highest NO flux for non-layered composites in 24 h. Additionally, a comparative study on NO flux modulation *via* the choice of metal nanoparticles is shown. Furthermore, mouse fibroblast cell viability when exposed to leachates from the polymer metal composites was dependent on (1) the design of the polymer composite where the layered approach performed better than non-layered composites (2) diffusion of metal nanoparticles from the composites plays a key role. Antibacterial activity on methicillin-resistant *Staphylococcus aureus* was also dependent on individual metal nanoparticles and flux levels in a 24 h *in vitro* CDC bioreactor study. Therefore, the study establishes the need for a layered polymer metal composite strategy that synergizes NO flux without negatively affecting biocompatibility.

1. Introduction

Nitric oxide (NO) is a key gaseous free radical messenger molecule that regulates various physiological pathways.[1] In mammals, NO is produced endogenously by the nitric oxide synthases (NOS) as a byproduct of the conversion of L-arginine to L-citrulline.[2] Bacterial infection within the body activates a cytokine surge which stimulates macrophages to upregulate NO production.[2] In turn, NO *via* multiple mechanisms can counter bacterial infection, including membrane destabilization, lipid peroxidation, DNA damage, *etc.* Several synthetic NO donors have been synthesized to mimic endogenous NO release to

fight infection. *S*-Nitrosothiols (RSNO) are of particular interest due to their physiological relevance as NO transporter within the body.[3] The NO release from RSNO is triggered by multiple stimuli, such as heat, light, and metal ions.[3] Various RSNOs have been incorporated within the polymer coating system to develop NO-releasing antibacterial surfaces.[4–15] Previous studies have shown that eradication of adhered bacteria from NO-releasing surfaces is dose-dependent on NO release or NO flux from the surface.[16] Nichols *et al.* also posited that the biocidal activity of NO is not immediate upon the surface adhesion of bacteria.[16] Therefore, optimization of NO release or NO flux is desirable for various applications.

One strategy that can be employed to increase initial NO fluxes to tackle the bacterial onslaught is *via* metal ions to catalyze the decomposition rate of RSNOs. Trace copper ions in solutions have been shown to affect RSNO decomposition.[17] Dicks *et al.* have demonstrated that reducing Cu(II) ions to Cu(I) ions is key to the catalytic process.[18] Several other transition

[a] *School of Chemical, Materials & Biomedical Engineering, University of Georgia, 302 E Campus Road, Suite 2212, GA 30605, Athens 30602, USA.*
E-mail: ejbrisbois@uga.edu

[b] *Department of Pharmaceutical & Biomedical Sciences, University of Georgia, Athens 30602, USA*

metal ions have been identified to exhibit catalytic activity towards RSNO decomposition to release NO.[19,20] Some of the metal ions are abundantly present in the physiological environment as metal centers of metalloenzymes or biological molecules such as hemoglobin and are known to partake in NO regulation.[21,22] Several blood-contacting metallic implant interfaces may generate NO which helps in resolving thrombosis or tissue overgrowth.[7,19] From a tunability perspective, metal ions can alter flux levels to create favorable conditions that can prevent or eradicate infection at device surfaces.[9,23,24] Survey studies on transition metal-mediated catalytic decomposition of RSNO were conducted either in the metal salt solution phase[20] or using a bare metal surface in the presence of RSNO solution (such as *S*-nitroso-*N*-acetylpenicillamine, SNAP).[19]

In this study, several metal nanoparticles, including Cu, silver (Ag), zinc (Zn), iron (Fe), and nickel (Ni), are incorporated within a medical-grade polymer matrix along with an RSNO, SNAP. The catalytic decomposition of SNAP *via* the transition metal nanoparticles is relevant to polymer coating systems and provides insights into the metal-mediated tunability of NO fluxes. From a clinical standpoint, the polymer-metal composites (PMC) reported herein could be used for various biomedical applications, including infection-resistant or thrombus-resistant surfaces. A major focus of the present work is to find how the choice of metal nanoparticles incorporated in the polymer surface design system may affect the biological response towards mammalian cells or bacterial cells. The NO flux was measured using the gold-standard chemiluminescence-based NO analyzer, leaching of metals and NO donor was studied using spectroscopic techniques. The biological response of mammalian cells and bacterial cells was also surveyed. The catalytic NO flux generated and the intrinsic properties of the metal nanoparticles may help design surface properties tailored for specific biomedical applications.

2. Experimental section

2.1. Materials

Sodium nitrite (NaNO$_2$), ethylenediaminetetraacetic acid (EDTA), phosphate buffer saline (PBS) powder, hydrochloric acid (HCl), sulfuric acid (H$_2$SO$_4$), methanol ($>$99.8%), acetone ($>$99.5%), brain heart infusion (BHI) broth and agar, and zinc nanopowder (40–60 nm, $>$99%) were all purchased from Sigma-Aldrich (St. Louis, MO, USA). *N*-Acetyl-ᴅ-penicillamine (NAP) was purchased from PharmaBlock Sciences Inc. (Hatfield, PA). Reduced glutathione (GSH) was purchased from Gold Biotechnology (St. Louis, MO, USA). All other metal nanopowders, silver (50–60 nm), iron (35–45 nm), copper (40–60 nm), and nickel (40–60 nm), zinc (40–60 nm) were purchased from SkySpring Nanomaterials (Houston, TX, USA). A modified Griess reagent kit was purchased from Invitrogen *via* ThermoFisher Scientific. Carbosil 2080A polymer pellets were purchased through DSM. Mouse fibroblast cells (3T3, CRL-1658) and methicillin-resistant *Staphylococcus aureus* (ATCC BAA 41) were obtained through the American Type Culture Collection (ATCC, Manassas, VA, USA). Dulbecco's modified

Eagle's medium (DMEM) and penicillin-streptomycin were purchased through Gibco (Fisher Scientific, Waltham, MA, USA). Fetal bovine serum (FBS) for cell culture maintenance was purchased from VWR. Cell culture counting (CCK-8) kit was obtained through Enzo Life Sciences (Farmingdale, NY, USA).

2.2. SNAP and GSNO synthesis

S-nitroso-*N*-acetylpenicillamine (SNAP) was synthesized by modifying an established protocol. First, equal concentrations of NAP and NaNO$_2$ were added to deionized water and methanol containing 1 M HCl and 1 M H$_2$SO$_4$. Next, the solution was stirred for 30 min at room temperature (RT) and then transferred to an ice bath for 6 h until SNAP crystals precipitated. SNAP crystals were then collected *via* vacuum filtration and dried in a desiccator for 24 h. During the whole process, the setup was protected from light to prevent the conversion of SNAP to NO. Finally, the yield and purity of SNAP samples were measured before storage at −20 °C.

S-nitrosoglutathione (GSNO) was synthesized by first dissolving glutathione (GSH) in 2 M HCl. The solution was cooled in an ice bath for 10 min before adding NaNO$_2$. After 40 min in the ice bath, chilled acetone was added to the solution and stirred until a light pink precipitate appeared. The precipitate was rinsed with chilled acetone and deionized water and dried in a vacuum desiccator for 24 h away from light.

2.3. PMC fabrication

The preparation of non-layered films consisted of sequential mixing stages adding in each component of the film until a dissolved, uniform solution was observed for film casting. The Carbosil films were prepared with 50 mg of Carbosil 2080A per 1 mL of THF in a vial while stirring for 4 hours. For the non-layered films, the desired metal nanoparticle, at the mass correlating to 1 wt% of the final film, was mixed into solution using a stir plate, vortex, and sonication until the uniform suspension was achieved. After mixing, SNAP was added, correlating to 10 wt% of the final film composition in the case of all SNAP-Carbosil films, and allowed to mix using a stir plate and vortex. The Carbosil solutions and SNAP-Carbosil solutions were cast into a Teflon mold (diameter = 2.54 cm) and dried overnight in darkness.

The preparation of layered films was initiated by mixing 50 mg of Carbosil per 1 mL of THF in a vial while stirring for 4 hours. After stirring, for SNAP-Carbosil films, SNAP was added at a concentration of 10 wt% mixing with the use of a stir plate and vortex. Carbosil and SNAP-Carbosil solutions were then cast into the Teflon mold (diameter = 2.54 cm) and dried overnight in darkness. The resulting films were hole punched with a diameter of 5/16 inches and prepared for dip-coating. All SNAP films were washed with methanol to dissolve SNAP crystals on the surface of the film. The dip-coat solution was also 50 mg of Carbosil 2080A per 1 mL of THF with 8 mg (1 wt%) of metal (Ag, Cu, Fe, Ni, or Zn) added and sonicated for 15 minutes. All metal-containing films were dip-coated once in these solutions and dried overnight. Control films were

dip-coated once in Carbosil solution (50 mg Carbosil per 1 mL of THF) with no metals and dried overnight.

2.4. SEM/EDS

The surface and cross-sectional morphology of the PMCs were imaged using field emission scanning electron microscopy (SEM, FEI Teneo, FEI Co.) at an accelerating voltage of 10.0 kV and a working distance of 10.0 mm. The samples were coated with 10 nm of gold under vacuum by a Leica sputter coater before imaging. The samples were further characterized for elemental content and distribution using adjunct energy-dispersive X-ray spectroscopy (EDS, Oxford Instruments).

2.5. Contact angle

The static contact angle for all films was measured using an Ossila Goniometer with 5 μL droplets of deionized water. Each film was mounted on a glass slide during contact angle measurement. The films were thoroughly dried using Kimwipes and air between each recorded measurement.

2.6. NO release measurement

Nitric oxide release from the PMC was measured using previously established methods using a chemiluminescence-based nitric oxide analyzer (Zysense Sievers NOA 280i, Boulder, CO).[6] The PMC films were placed in NOA cells immersed in 0.01 M PBS (pH 7.4) at a temperature of 37 °C. To measure the transition metal nanoparticle-mediated catalytic decomposition of SNAP in dry conditions at RT, the samples were placed inside NOA cells without any buffer. In the NOA setup, NO released from the composite films was continuously purged from the sample cell and swept from the headspace by N_2 sweep gas and bubbler. The NOA sample cells were made of amber glass to protect the SNAP contained within composite films from photocatalytic degradation. The N_2 flow rate was set at 200 mL min^{-1}, and the chamber pressure and oxygen pressure were 6 Torr and 5.8–6.2 psi, respectively. The NO release measured was converted to NO surface flux and normalized by the surface area of the PMC films. The experiments were replicated at least 3 times.

2.7. SNAP diffusion

The SNAP-containing PMCs were soaked in 2 mL 0.01 M PBS inside vials and stored at 37 °C for 24 h. At various time points (1, 4, 8, 12, and 24 h), SNAP diffused into the PBS buffer was measured spectroscopically at 340 nm. SNAP shows characteristic maxima at 340 nm and 590 nm, which corresponds to π → π* and n_N → π* transitions of the S–NO bond.[25] The PBS buffer with EDTA was used as blank. All experiments were conducted in triplicates.

2.8. Metal ion diffusion

Leachates of Cu, Ag, Ni, Zn, and Fe containing CarboSil samples were prepared by soaking the samples in 0.01 M PBS for 24 h. The diffusion of metal ions from the samples was analyzed by utilizing PerkinElmer 8300 Inductively Coupled Plasma Optical Emission Spectrophotometer (ICP-OES).

2.9. CCK-8 assay

The CCK-8 assay was employed to determine the viability of 3T3 mouse fibroblast cells in the presence of leachates from PMC. The leachates were prepared by soaking PMC samples in complete DMEM (containing 10% FBS and 5% pen-strep) for 24 h. Mouse fibroblast cells were prepared in complete DMEM at a seeding density of 1×10^4 cells per mL in a 96-well plate. After 24 h, the media was replaced with media containing the leachates and incubated at 37 °C in a humidified atmosphere with 5% CO_2. After 24 h incubation, 10% CCK-8 solution prepared in media was added to each well and incubated for 3 h. The CCK-8 kit has a highly water-soluble tetrazolium salt, WST-8 [2-(2-methoxy-4-nitrophenyl)-3-(4-nitrophenyl)-5-(2,4-disulfophenyl)-2H-tetrazolium monosodium salt], which is reduced by dehydrogenases in viable cells to form formazan, an orange-colored product, which can be spectrophotometrically detected at 450 nm wavelength. The results are reported as cell viability relative to the control, which did not contain any leachates. All experiments were conducted in triplicates at different cell passages.

2.10. Griess assay

Total nitrites present in the leachates were determined using Griess Assay. A Griess Reagent Kit (Molecular Probes, OR) was employed to quantify nitrite concentrations of the leachates prepared in complete DMEM without phenol red. The PMC samples were soaked in complete DMEM (-phenol red) for 24 h at 37 °C. After 24 h, the leachates were collected and prepared for nitrite quantification according to the manufacturer's protocol. Briefly, equal volumes of 0.1% N-(1-naphthyl)ethylenediamine dihydrochloride and 1% sulfanilic acid were added to form the Griess reagent. The nitrite-containing leachates were added to the Griess reagent in a 96-well plate and incubated for 30 min. Next, the absorbance was measured at 548 nm using a multi-plate reader (BioTek, Agilent, Santa Clara, CA, USA). Calibration curves were previously constructed using sodium nitrite in deionized water.

2.11. Antibacterial efficacy

The antibacterial activity of the PMC samples was evaluated against MRSA (ATCC BAA 041) in a CDC bioreactor model. MRSA was inoculated in BHI media at 37 °C for 10 h at 150 rpm. The MRSA culture was centrifuged at 2500 rpm for 7 min and washed with 0.01 M PBS for the experiment. Finally, the culture was adjusted to a 10^6 CFU per mL concentration in 10% BHI. The samples were placed in sample holders inside the bioreactor vessel. The bacterial solution was introduced within the bioreactor vessel and stirred at 200 rpm for 1 h at 37 °C. After 1 h, the stirring was reduced to 120 rpm, and 10% BHI media flowed at a rate of 1.6 mL min^{-1} at 37 °C. After 24 h, the samples were collected and gently rinsed in 0.01 M PBS to eliminate any loosely attached bacteria or planktonic bacteria. The adhered bacteria on the surface of the samples were detached using a homogenizer at 25 000 rpm for 60 s, followed by vortexing for another 60 s in 0.01 M PBS. The resulting bacterial solution was serially diluted to desired concentrations *via* pipetting. Final serial dilutions were plated using a spiral

plater (Eddy Jet, IUL SA) on BHI agar plates. Bacterial colonies were counted on an automatic colony counter (SphereFlash®) normalized against samples by surface area (CFU/cm²). The following equation calculated the percentage reduction of viable adhered bacteria where $C = \dfrac{\text{CFU}}{\text{cm}^2}$.

$$\text{Reduction efficiency (\%)} = \frac{C_{\text{control}} - C_{\text{sample}}}{C_{\text{control}}} \times 100$$

3. Results and discussion

3.1. Fabrication and characterization

Previous studies on the catalytic effect of transition-metal ions on RSNOs have been conducted in the solution phase or using a bare-metal stent surface.[19,20] In both cases, solutions of RSNO was used against metal salts or bulk metal surface.[19,20] While previous reports are insightful towards metal-endogenous RSNO interaction within the body, RSNO and metal interaction within a polymer composite have not been explored. Therefore, the experimental approach was kept uniform by the use of a widely used standard medical-grade polymer, CarboSil, which is a blend of polycarbonate-urethane with a mix of poly(dimethylsiloxane) as well as a hard segment of methylene diphenyl isocyanate (MDI) and used for gasotransmitter delivery.[13,26] The size of the metal nanoparticles was kept consistent within 40–60 nm (see Section 2.1).

For fabrication, 50 mg mL⁻¹ Carbosil was dissolved in THF. As a result, SNAP incorporated was 10 wt% of the final film. To maintain uniformity, the concentration of metal nanoparticles was 1 wt% of CarboSil for all metals. Two design strategies were employed during PMC fabrication. The first method incorporated SNAP and metal nanoparticles in a single CarboSil composite. In the second method, SNAP was incorporated first in a CarboSil composite (CarboSil-SNAP), and then, metal-CarboSil was dip-coated onto CarboSil-SNAP. Therefore, the second fabrication method led to a layered composite structure where SNAP and metal nanoparticles did not reside in the same composite (Fig. 1). The rationale behind a layered structure was to investigate the catalytic capability of the metal nanoparticles as water infiltrated the polymer system leading to SNAP diffusion or metal diffusion. SNAP diffusion is known to be slower in low-water uptake polymers.[6] SNAP doping at 10 wt% leads to orthorhombic crystal formation within the bulk of CarboSil stabilizing SNAP within the polymer matrix.[27] The samples prepared are compiled in Table 1. Polymers without SNAP are referred to as w/o SNAP (without SNAP) in figures, captions, or text. Non-layered films without SNAP were found to have a thickness of ∼0.19 mm, while those with SNAP increased to ∼0.21 mm on average. A similar trend was observed for layered films where non-SNAP films measured 0.33 mm thickness, with SNAP layered films having a thickness of 0.35 mm. Layered films *via* dip coating cause a thickness increase of 0.14 mm. The presence of a polymer layer topcoat has been shown to increase the film's thickness and reduces SNAP and NO diffusion from the polymer matrix.[6] These differences in thickness were accounted for *via* data with respect to the surface area to normalize all data provided between film types.

Polymer Metal Composite Design

Fig. 1 Fabrication scheme of polymer–transition metal composites (PMC).

Table 1 Compilation of the samples fabricated and their annotations; DC indicates Dip-coated samples

	Metal NP	Non-SNAP	SNAP
Non-layered	Control	CarboSil	SNAP
	Fe	Fe	SNAP-Fe
	Ag	Ag	SNAP-Ag
	Cu	Cu	SNAP-Cu
	Zn	Zn	SNAP-Zn
	Ni	Ni	SNAP-Ni
Layered	Control	DC-CarboSil	DC-SNAP
	Fe	DC-Fe	DC-SNAP-Fe
	Ag	DC-Ag	DC-SNAP-Ag
	Cu	DC-Cu	DC-SNAP-Cu
	Zn	DC-Zn	DC-SNAP-Zn
	Ni	DC-Ni	DC-SNAP-Ni

3.2. Surface properties

The surface properties of the PMC were characterized by SEM, EDS, and contact angle measurements. As shown in Fig. 2, SEM images provide insight into the changes in surface topography when metal nanoparticles are incorporated. The change in surface morphology could influence surface wettability and, therefore, water availability within the polymer matrix. In most cases, the layered PMC had similar topography compared to the non-layered topography. It is highly likely that in non-layered PMC, the interaction between SNAP and metal ions during the solvent evaporation phase could affect the surface structure. Premature decomposition of RSNO by metals that exhibit a stronger catalytic effect can lead to a 'pothole' like appearance on the surface, possibly due to NO release during the polymer curing process as observed for Zn (Fig. 2R). While the same cannot be said for Cu, which elicits a very strong catalytic effect, there is a distinct difference in the surface topography due to the presence or absence of SNAP. This may be explained because Cu(I) usually

Fig. 2 Surface topography of the non-layered PMC (A, B, E, F, I, J, M, N, Q, R, U and V) and layered PMC (C, D, G, H, K, L, O, P, S, T, W and X). $N \geq 3$.

catalyzes RSNO decomposition and requires a reducing agent to attain a relatively unstable Cu(I) state. Due to a lack of interaction with SNAP, the surface topography of layered PMC is similar. EDS was employed to confirm the presence of metal nanoparticles and

SNAP. Fig. 3 shows that all the metal nanoparticles had homogenous distribution within the CarboSil polymer matrix.

Contact angle as a surface change parameter can provide insights into wettability changes due to layered or non-layered

Fig. 3 Representative images of EDS maps of the metals (Fe, Ag, Cu, Zn, Ni) present in the layered PMCs for films with and without (w/o) SNAP. $N \geq 3$.

PMC design. A change in surface topography may stimulate a change in surface wettability. Surface modification affected by the presence of metal nanoparticles or metal-SNAP interaction may eventually affect the NO release profile or biological responses. As seen in Fig. 4, the incorporation of SNAP significantly ($p < 0.05$) changed the wettability of control CarboSil, CarboSil-Ag, CarboSil-Zn, and CarboSil-Ni. Except for CarboSil-Ni, the hydrophobicity of the surfaces decreased. Similarly, for layered PMC, significant changes in surface hydrophobicity were observed for control DC-CarboSil, DC-CarboSil-Fe, DC-CarboSil-Zn, and DC-CarboSil-Ni upon SNAP incorporation in the inner layer. Therefore, the results suggest that incorporating metal nanoparticles or SNAP can vary the surface hydrophobicity of the CarboSil polymer system.

3.3. NO release kinetics and SNAP diffusion

The catalytic activity of the metal nanoparticles present within the CarboSil matrix was evaluated by measuring NO using a chemiluminescence-based NO analyzer (Sievers). Metal ions catalyze the decomposition of RSNO into NO and thiyl radicals.[19] From Fig. 5A and B, we observe that catalytic NO release under physiological conditions depends on metal nanoparticles. The presence of Cu, Fe, Ag, Zn, and Ni nanoparticles showed a catalytic burst release by varying degrees. Previous studies have shown metal ions play a significant role in the catalytic decomposition of RSNO such as Cu^+, Fe^{2+}, and subsequent reduced Fe^{3+}, Ag^+, Zn^{2+}, and Ni^{2+}.[19,20] These metal ions exhibit distinct valence states contributing to their catalytic activity. For example, Cu^+ have been observed to participate in RSNO decomposition reactions, wherein they undergo redox transformations.[18] Similarly, Fe^{2+} is known to play a catalytic role in RSNO decomposition, while their subsequent reduced form, Fe^{3+}, further contributes to the decomposition process by reduction to Fe^{2+} by trace thiols.[20]

Thus, the design of the PMC plays an important factor in controlling the catalytic NO flux. All the samples were pre-soaked in 0.01 M PBS for 1 h before the NO release measurement. As expected, layered PMC had, in general, lower fluxes when compared to non-layered PMC. For comparison, the NO surface flux of non-layered SNAP-Fe is $68 \pm 8 \times 10^{10}$ mol cm^{-2} min^{-1}, whereas DC-SNAP-Fe surface flux is $7 \pm 3 \times 10^{10}$ mol cm^{-2} min^{-1}. The reduced surface flux that is uniform among non-layered PMC is due to its bilayer design, preventing SNAP and metal ions from coming into direct contact. Secondly, the additional layer provides a physical barrier to water infiltration to the SNAP within the CarboSil layer. For layered PMC, the catalytic event can occur when SNAP diffuses from the inner polymer onto the outer layer containing metal nanoparticles. In previous studies, Cu was shown to retain a catalytic effect when present as a dip-coated outer layer.[9,23] For non-layered PMC, stabilized NO surface flux differs by metal contents by the following order: SNAP-Fe > SNAP-Zn > SNAP-Ni > SNAP-Cu > SNAP-Ag. It is interesting to note that the catalytic flux of Cu is lower than Fe, Zn, or Ni. For flux calculations, stabilized flux was considered. However, as shown in Fig. 5C and D, when total NO release at 1 h time point ([NO$_{1h}$] in moles) is considered, Cu has the highest catalytic activity, which aligns with the literature.[19,20] For layered PMC, the stabilized NO surface flux order was: DC-SNAP-Cu > DC-SNAP-Ni > DC-SNAP-Zn > DC-SNAP-Ag > DC-SNAP-Fe. It becomes evident that in the absence of a coated layer, SNAP-Cu resorts to a high burst release before attaining flux stability. Therefore, during the design of polymer surfaces during any application, the layering or non-layering of the composite should be under consideration.

The SNAP diffusing from the PMC can affect the NO surface flux due to its interaction with metal nanoparticles. While SNAP can directly interact with metal nanoparticles in non-layered PMC, it must diffuse out to the topcoat on the layered PMC. The data in Fig. 5E and F observe a higher percentage of SNAP diffusion for non-layered PMC. The metal composites that display higher

Fig. 4 Contact angle of (a) and (c) non-layered and (b) and (d) layered PMC. Significance is indicated by asterisks where * is $p < 0.05$, ** is $p < 0.01$, *** is $p < 0.001$ Data is represented as mean ± standard deviation. $N \geq 3$.
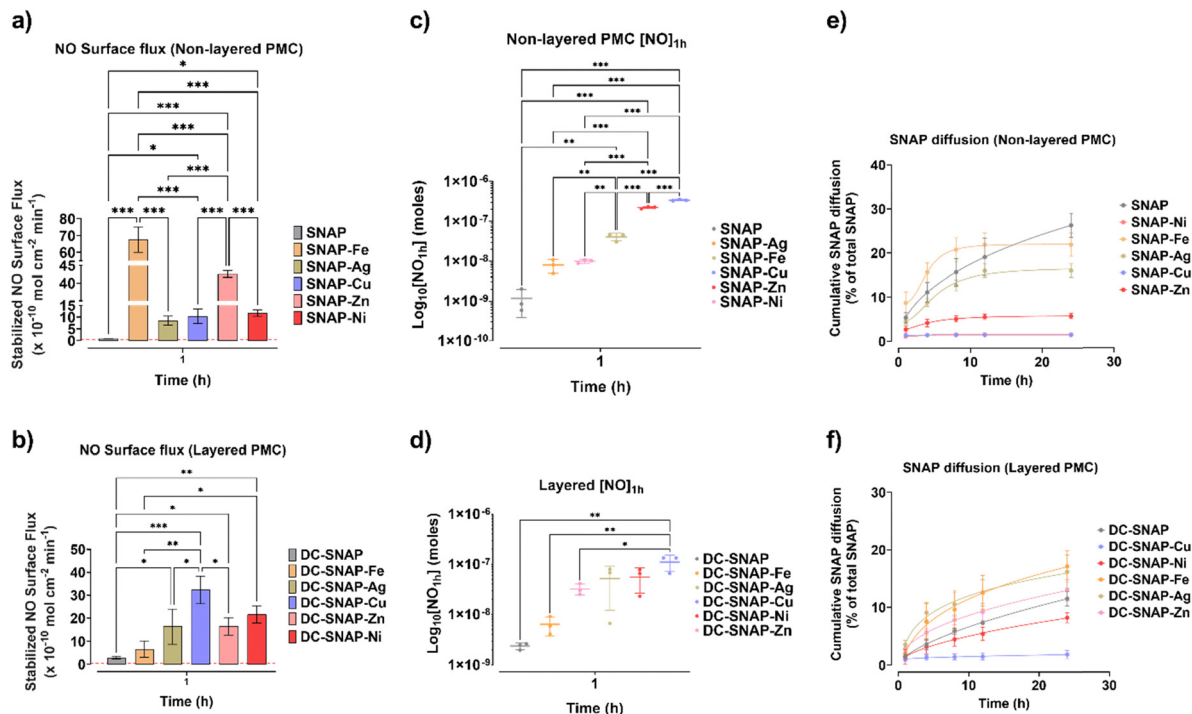
Fig. 5 Graphs depicting transition metal-mediated catalytic stabilized NO surface flux from SNAP decomposition within CarboSil matrix in (a) non-layered and (b) layered PMC after 1 h time point. Moles of NO released after 1 h is shown for the (c) non-layered and (d) layered PMC. SNAP diffusion as cumulative % of total SNAP is shown for the (e) non-layered and (f) layered PMC. Significance is indicated by asterisks where * is $p < 0.05$, ** is $p < 0.01$, *** is $p < 0.001$. Data represented as mean $\pm$ standard deviation. $N \geq 3$.

catalytic NO release have lower SNAP diffusing into the solution. Before it can diffuse out, SNAP is decomposed by metals such as Cu, Zn, or Ni. Overall, the non-layered PMC had a higher cumulative SNAP diffusion percentage than the layered PMC. It may be vital as SNAP diffused from the composite may also exert oxidative stress on surrounding cells. Therefore, the addition of metal nanoparticles improves the tunability of NO surface flux and may also allow control of SNAP diffusion.

3.4. Effect on mammalian cell viability

The choice of a metal nanoparticle and the design is important in understanding the tunability of NO flux mediated by

transition metal nanoparticles. Cytotoxicity imparted by the leachates/diffusates from the PMC is critical in determining tailored NO flux for various applications. From Fig. 6, it is evident that while non-layered Cu and Zn w/o SNAP do not cause a reduction in viable mouse fibroblast cells, non-layered SNAP-Cu and SNAP-Zn does. Reduction in viable cells is also observed for SNAP control, implying that any metal nanoparticle leaching is not responsible for eliciting a cytotoxic effect. Table 2 provides ICP-OES data of metals leached out of layered PMC. The interaction between SNAP and Cu, Zn, or Ni (to some extent) could cause a cytotoxic effect. Interestingly, higher leaching of Cu ($16.7 \ \mu g \ g^{-1}$) and Zn ($21.0 \ \mu g \ g^{-1}$) from SNAP-Cu and SNAP-Zn,
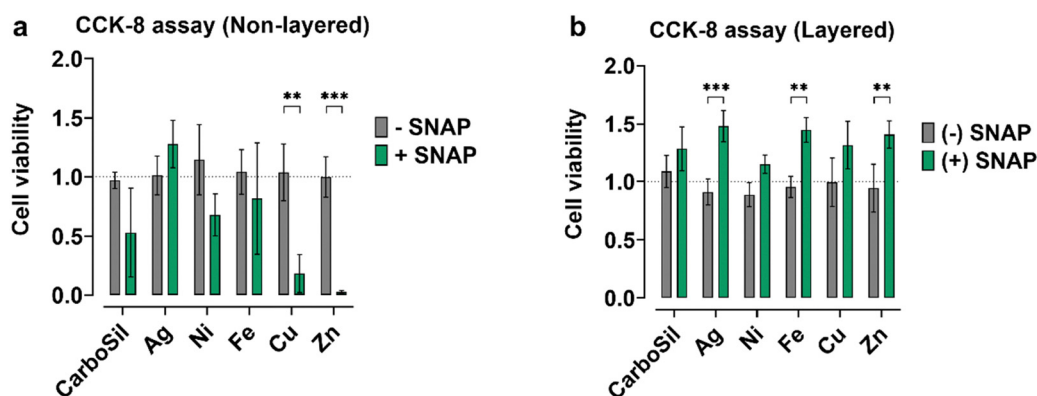

Fig. 6 Graphs depict the cell viability of mouse fibroblast cells when exposed to the leachates from (a) non-layered PMC and (b) layered PMC. Significance is indicated by an asterisk where ** is $p < 0.01$, *** is $p < 0.001$. Data is represented as mean $\pm$ standard deviation. $N \geq 3$ passages of cells.

respectively, correspond to highly reduced amounts of viable cells. Cytotoxicity of Cu and Zn nanoparticles is known to be concentration-dependent.[28,29] Complete DMEM contains FBS, which has albumin and other proteins are constituents. The NO at a high concentration can nitrosate thiols present in protein.[30,31] High NO concentration or SNAP leachates in the DMEM media can also deplete glutathione in cells, which protects cells from oxidative stress.[32] The cytotoxic effects completely disappear in the case of layered PMC design compared to non-layered Cu & Zn containing PMC. Cell viability increased significantly ($p < 0.05$) from its non-SNAP counterparts for DC-SNAP-Ag, DC-SNAP-Fe, and DC-SNAP-Zn. However, it is unclear if the increased cell viability results from NO or moderate oxidative products generated in the leachate media, which drives cell proliferation. Gooch *et al.* have shown that oxidants in media are responsible for increased cell viability and not the presence of NO.[33] However, results from this experiment suggest the importance of having a layered PMC design where NO flux, SNAP diffusion, and nanoparticle leachate diffusion are comparatively lower than non-layered PMC, which, in turn, affects the cell viability of mouse fibroblast cells.

3.5. *In vitro* CDC bioreactor infection model

The NO produces reactive nitrogen species (RNS) such as dinitrogen trioxide (N_2O_3), nitrogen dioxide (NO_2), or peroxynitrite ($OONO^-$), which can oxidize membrane proteins, cause lipid peroxidation or DNA cleavage.[34,35] As a free radical, NO can react with other free radicals, such as superoxide and hydrogen peroxide, for reactive oxygen/nitrogen species.[34] Therefore, for various biomedical applications, tunability is an important factor in controlling the infection resistance of medical device surfaces. For the antibacterial study, the layered PMC was considered owing to the cytotoxicity of some non-layered PMC. Methicillin resistant *S. aureus* (MRSA) is a virulent strain that can release aggressive toxins and is commonly involved in most medical device-related infections.[36] Fig. 7 depicts the log reduction of viable MRSA when exposed to the PMC in a 24 h CDC bioreactor study. A bioreactor study is a robust experimentation where bacterial biofilm and cell viability are evaluated under shear stress.[37] In the current study, except DC-SNAP-Cu, which has a log reduction of 0.78, the presence of other metals (at 1 wt%) with SNAP does not effectively inhibit bacterial cell viability when compared to SNAP control. SNAP-containing layered PMCs have higher bacterial reduction efficiency compared to non-SNAP samples. Between SNAP-containing and non-SNAP-containing PMC, DC-SNAP-Ag does not demonstrate any
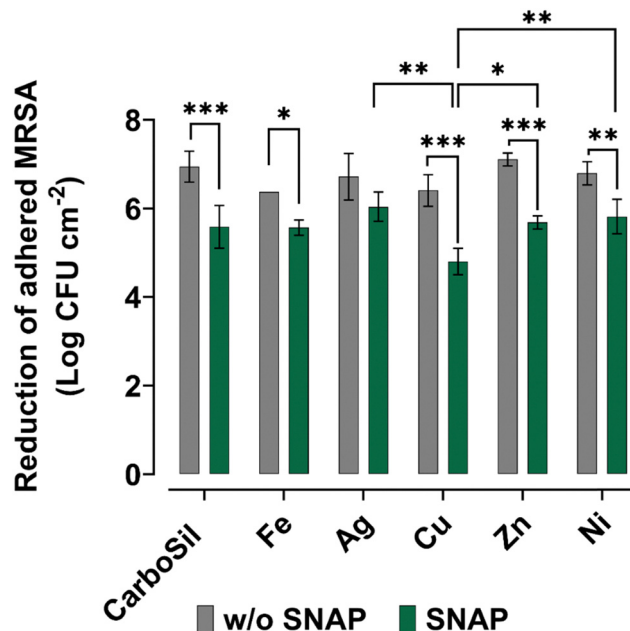

Fig. 7 Antibacterial activity of the layered PMC samples when exposed to MRSA for 24 h at 37 °C in a CDC bioreactor. Significance is indicated by asterisks where * is $p < 0.05$, ** is $p < 0.01$, *** is $p < 0.001$. Data is represented as mean ± standard deviation. $N \geq 3$.

significant difference in the log reduction. Moreover, DC-SNAP-Zn, DC-SNAP-Ni, and DC-SNAP-Fe exert an antibacterial effect comparable to the catalytic decomposition of RSNO within the polymer matrix (1.26, 1.12, 1.37 log reduction). Some metal nanoparticles, such as Cu, are also known to exert an antibacterial effect.[38] Therefore, combining NO flux and the inherent antimicrobial property of metals can be a potent surface strategy to counter medical device infection.

4. Conclusion

The tunability of NO flux of NO-releasing medical-grade polymer surfaces is desirable for biomedical applications. In this study, transition metal nanoparticles of Cu, Ag, Fe, Zn, and Ni are employed in a non-layered and layered PMC to decompose SNAP catalytically. The NO release survey of these five metal nanoparticles shows that catalytic NO release varies by choice of metal. Cu showed the highest catalytic activity, followed by Zn and Ni when layered PMC was considered. Non-layered PMC with SNAP, except Ag, showed significant cytotoxicity toward mouse fibroblast cell lines. Thus, demonstrating that layered PMC is more suitable for biomedical applications. In addition, the antibacterial activity of the layered PMC, evaluated in a CDC bioreactor model, showed that Cu-containing composites were most effective in reducing adhered bacterial viability (2.13 log reduction). The results from this study may shape the premise on which tunable NO-releasing surfaces can be developed.

Conflicts of interest

There are no conflicts to declare.

Table 2 ICP-OES measurement of metal ions leached out of the layered PMC and non-layered PMC

Metal nanoparticles	Layered		Non-layered	
	w/o SNAP ($\mu g\ g^{-1}$)	SNAP ($\mu g\ g^{-1}$)	w/o SNAP ($\mu g\ g^{-1}$)	SNAP ($\mu g\ g^{-1}$)
Ag	<0.12	<0.12	<0.30	0.79
Fe	<4.74	<4.74	<0.96	<0.95
Cu	0.18	0.11	<0.25	16.7
Zn	<0.42	<0.42	0.69	21.0
Ni	<0.44	<0.44	1.36	12.0

Acknowledgements

References

1 K. Ghimire, H. M. Altmann, A. C. Straub and J. S. Isenberg, Nitric oxide: what's new to NO?, *Am. J. Physiol.: Cell Physiol.*, 2017, **312**(3), C254–C262.

2 B. N. Gantner, K. M. LaFond and M. G. Bonini, Nitric oxide in cellular adaptation and disease, *Redox Biol.*, 2020, **34**, 101550.

3 D. A. Riccio and M. H. Schoenfisch, Nitric oxide release: part I. Macromolecular scaffolds, *Chem. Soc. Rev.*, 2012, **41**(10), 3731.

4 D. A. Riccio, K. P. Dobmeier, E. M. Hetrick, B. J. Privett, H. S. Paul and M. H. Schoenfisch, Nitric oxide-releasing S-nitrosothiol-modified xerogels, *Biomaterials*, 2009, **30**(27), 4494–4502.

5 S. Bhagchandani, J. A. Johnson and D. J. Irvine, Evolution of Toll-like receptor 7/8 agonist therapeutics and their delivery approaches: From antiviral formulations to vaccine adjuvants, *Adv. Drug Delivery Rev.*, 2021, **175**, 113803.

6 E. J. Brisbois, H. Handa, T. C. Major, R. H. Bartlett and M. E. Meyerhoff, Long-term nitric oxide release and elevated temperature stability with S-nitroso-N-acetylpenicillamine (SNAP)-doped Elast-eon E2As polymer, *Biomaterials*, 2013, **34**(28), 6957.

7 E. J. Brisbois, M. Kim, X. Wang, A. Mohammed, T. C. Major, J. Wu, J. Brownstein, C. Xi, H. Handa, R. H. Bartlett and M. E. Meyerhoff, Improved Hemocompatibility of Multilumen Catheters via Nitric Oxide (NO) Release from S-Nitroso-N-acetylpenicillamine (SNAP) Composite Filled Lumen, *ACS Appl. Mater. Interfaces*, 2016, **8**(43), 29270–29279.

8 R. Devine, M. J. Goudie, P. Singha, C. Schmiedt, M. Douglass, E. J. Brisbois and H. Handa, Mimicking the Endothelium: Dual Action Heparinized Nitric Oxide Releasing Surface, *ACS Appl. Mater. Interfaces*, 2020, **12**(18), 20158–20171.

9 M. E. Douglass, M. J. Goudie, J. Pant, P. Singha, S. Hopkins, R. Devine, C. W. Schmiedt and H. Handa, Catalyzed Nitric Oxide Release Via Cu Nanoparticles Leads to an Increase in Antimicrobial Effects and Hemocompatibility for Short Term Extracorporeal Circulation, *ACS Appl. Bio Mater.*, 2019, **2**(6), 2539–2548.

10 M. J. Goudie, J. Pant and H. Handa, Liquid-infused nitric oxide-releasing (LINORel) silicone for decreased fouling, thrombosis, and infection of medical devices, *Sci. Rep.*, 2017, **7**(1), 13623.

11 M. J. Goudie, P. Singha, S. P. Hopkins, E. J. Brisbois and H. Handa, Active Release of an Antimicrobial and Antiplatelet Agent from a Nonfouling Surface Modification, *ACS Appl. Mater. Interfaces*, 2019, **11**(4), 4523–4530.

12 S. P. Hopkins, J. Pant, M. J. Goudie, C. Schmiedt and H. Handa, Achieving Long-Term Biocompatible Silicone via Covalently Immobilized S-Nitroso- N-acetylpenicillamine (SNAP) That Exhibits 4 Months of Sustained Nitric Oxide Release, *ACS Appl. Mater. Interfaces*, 2018, **10**(32), 27316–27325.

13 A. Mondal, M. Douglass, S. P. Hopkins, P. Singha, M. Tran, H. Handa and E. J. Brisbois, Multifunctional S-Nitroso-N-acetylpenicillamine-Incorporated Medical-Grade Polymer with Selenium Interface for Biomedical Applications, *ACS Appl. Mater. Interfaces*, 2019, **11**(38), 34652–34662.

14 A. Mondal, P. Singha, M. Douglass, L. Estes, M. Garren, L. Griffin, A. Kumar and H. Handa, A Synergistic New Approach Toward Enhanced Antibacterial Efficacy via Antimicrobial Peptide Immobilization on a Nitric Oxide-Releasing Surface, *ACS Appl. Mater. Interfaces*, 2021, **13**(37), 43892–43903.

15 J. Pant, M. J. Goudie, S. M. Chaji, B. W. Johnson and H. Handa, Nitric oxide releasing vascular catheters for eradicating bacterial infection, *J. Biomed. Mater. Res., Part B*, 2018, **106**(8), 2849–2857.

16 S. P. Nichols and M. H. Schoenfisch, Nitric oxide-flux dependent bacterial adhesion and viability at fibrinogen-coated surfaces, *Biomater. Sci.*, 2013, **1**(11), 1151.

17 D. L. H. Williams, The mechanism of nitric oxide formation from S-nitrosothiols (thionitrites), *Chem. Commun.*, 1996, 1085–1091.

18 A. P. Dicks, H. R. Swift, D. L. H. Williams, A. R. Butler, H. H. AlSadoni and B. G. Cox, Identification of Cu+ as the effective reagent in nitric oxide formation from S-nitrosothiols (RSNO), *J. Chem. Soc., Perkin Trans. 2*, 1996, (4), 481–487.

19 C. W. McCarthy, R. J. Guillory, J. Goldman and M. C. Frost, Transition-Metal-Mediated Release of Nitric Oxide (NO) from S-Nitroso-N-acetyl-D-penicillamine (SNAP): Potential Applications for Endogenous Release of NO at the Surface of Stents Via Corrosion Products, *ACS Appl. Mater. Interfaces*, 2016, **8**(16), 10128.

20 A. Lutzke, A. C. Melvin, M. J. Neufeld, C. L. Allison and M. M. Reynolds, Nitric oxide generation from S-nitrosoglutathione: New activity of indium and a survey of metal ion effects, *Nitric oxide*, 2019, **84**, 16–21.

21 D. Giustarini, A. Milzani, R. Colombo, I. Dalle-Donne and R. Rossi, Nitric oxide and S-nitrosothiols in human blood, *Clin. Chim. Acta*, 2003, **330**(1–2), 85–98.

22 C. E. Cooper, Nitric oxide and iron proteins, *Biochim. Biophys. Acta*, 1999, **1411**(2–3), 290–309.

23 J. Pant, M. J. Goudie, S. P. Hopkins, E. J. Brisbois and H. Handa, Tunable Nitric Oxide Release from S-Nitroso-N-acetylpenicillamine via Catalytic Copper Nanoparticles for Biomedical Applications, *ACS Appl. Mater. Interfaces*, 2017, **9**(18), 15254–15264.

24 P. Singha, C. D. Workman, J. Pant, S. P. Hopkins and H. Handa, Zinc-oxide nanoparticles act catalytically and synergistically with nitric oxide donors to enhance antimicrobial efficacy, *J. Biomed. Mater. Res., Part A*, 2019, **107**(7), 1425–1433.

25 M. C. Frost and M. E. Meyerhoff, Controlled photoinitiated release of nitric oxide from polymer films containing S-nitroso-N-acetyl-DL-penicillamine derivatized fumed silica filler, *J. Am. Chem. Soc.*, 2004, **126**(5), 1348.

26 J. Pant, A. Mondal, J. Manuel, P. Singha, J. Mancha and H. Handa, H2S-Releasing Composite: a Gasotransmitter

Platform for Potential Biomedical Applications, *ACS Biomater. Sci. Eng.*, 2020, **6**(4), 2062–2071.

27 Y. Wo, Z. Li, E. J. Brisbois, A. Colletta, J. Wu, T. C. Major, C. Xi, R. H. Bartlett, A. J. Matzger and M. E. Meyerhoff, Origin of Long-Term Storage Stability and Nitric Oxide Release Behavior of CarboSil Polymer Doped with S-Nitroso-N-acetyl-D-penicillamine, *ACS Appl. Mater. Interfaces*, 2015, **7**(40), 22218.

28 B. Cao, Y. Zheng, T. Xi, C. Zhang, W. Song, K. Burugapalli, H. Yang and Y. Ma, Concentration-dependent cytotoxicity of copper ions on mouse fibroblasts in vitro: effects of copper ion release from TCu380A *vs.* TCu220C intra-uterine devices, *Biomed. Microdevices*, 2012, **14**(4), 709.

29 W. Song, J. Zhang, J. Guo, J. Zhang, F. Ding, L. Li and Z. Sun, Role of the dissolved zinc ion and reactive oxygen species in cytotoxicity of ZnO nanoparticles, *Toxicol. Lett.*, 2010, **199**(3), 389.

30 V. G. Kharitonov, A. R. Sundquist and V. S. Sharma, Kinetics of Nitrosation of Thiols by Nitric Oxide in the Presence of Oxygen, *J. Biol. Chem.*, 1995, **270**(47), 28158–28164.

31 K. A. Broniowska and N. Hogg, The chemical biology of S-nitrosothiols, *Antioxid. Redox Signaling*, 2012, **17**(7), 969.

32 M. W. Walker, M. T. Kinter, R. J. Roberts and D. R. Spitz, Nitric Oxide-Induced Cytotoxicity: Involvement of Cellular Resistance to Oxidative Stress and the Role of Glutathione in Protection, *Pediatr. Res.*, 1995, **37**(1), 41–49.

33 K. J. Gooch, C. A. Dangler and J. A. Frangos, Exogenous, basal, and flow-induced nitric oxide production and endothelial cell proliferation, *J. Cell. Physiol.*, 1997, **171**(3), 252.

34 F. Rong, Y. Tang, T. Wang, T. Feng, J. Song, P. Li and W. Huang, Nitric Oxide-Releasing Polymeric Materials for Antimicrobial Applications: A Review, *Antioxidants*, 2019, **8**(11), 556.

35 A. W. Carpenter and M. H. Schoenfisch, Nitric oxide release: part II. Therapeutic applications, *Chem. Soc. Rev.*, 2012, **41**(10), 3742.

36 Y. Zheng, L. He, T. K. Asiamah and M. Otto, Colonization of medical devices by staphylococci, *Environ. Microbiol.*, 2018, **20**(9), 3141–3153.

37 B. F. Gilmore, T. M. Hamill, D. S. Jones and S. P. Gorman, Validation of the CDC biofilm reactor as a dynamic model for assessment of encrustation formation on urological device materials, *J. Biomed. Mater. Res., Part B*, 2010, **9999B**, 128–140.

38 M. Raffi, S. Mehrwan, T. M. Bhatti, J. I. Akhter, A. Hameed, W. Yawar and M. M. Ul Hasan, Investigations into the antibacterial behavior of copper nanoparticles against *Escherichia coli*, *Ann. Microbiol.*, 2010, **60**(1), 75–80.